

**Supervised Telemanipulation Interface for Humanoid Driving**

A Thesis

Submitted to the Faculty

of

Drexel University

by

Karthikeyan Yuvaraj

in partial fulfillment of the

requirements for the degree

of

Master of Science in Electrical Engineering

December 2014

© Copyright 2014  
Karthikeyan Yuvaraj. All Rights Reserved.

## Acknowledgements

I am very much grateful for my advisor Dr. Paul Oh who taught me that anything is achievable through true dedication. I am very thankful to the members of the Drexel Autonomous Systems Lab, who has shown me kindness and inspired me in many ways. I would like to thank Dr. Christopher Rasmussen and Kiwon Sohn for their guidance and motivation.

## Table of Contents

LIST OF FIGURES .....	iv
1. Abstract .....	1
2. INTRODUCTION .....	2
3. RELATED WORK .....	5
4. SYSTEM OVERVIEW .....	9
4.1 Hubo 2+ .....	9
4.2 DRC-Hubo .....	9
5. Phases before Driving .....	11
5.1 Detecting the Interest Points in the Utility Vehicle .....	11
5.1.1 Locating the Floor .....	13
5.1.2 Locating the Steering Wheel .....	15
5.2 Approaching the Vehicle .....	15
5.2.1 Docking Phase .....	16
6. Driving a golf cart with a humanoid robot .....	18
6.1 Manipulating the Steering Wheel and the Pedal in a golf cart .....	19
6.2 Driving Interface for a Golf cart .....	21
6.3 Driving Experiment-1 .....	23
7. Driving with Polaris Ranger XP .....	27
7.1 Driving event in DRC-2013 .....	27
7.2 Sensor Head .....	27
7.3 Monitoring the state of the humanoid robot .....	29

7.4	Manipulating the Steering Wheel and the Pedal in the Polaris Ranger XP .....	30
7.5	Driving interface for the Polaris ranger XP .....	32
7.6	Driving Experiment-1 .....	34
8.	Conclusion .....	37
	BIBLIOGRAPHY .....	37
	APPENDIX A: COPYRIGHT INFORMATION .....	41

## List of Figures

2.1	Humanoid systems working to reduce further disaster in a factory. This is a concept picture from DARPA.....	2
2.2	Humanoid robot DRC-Hubo seated in a driving position.....	3
3.1	HRP-1,The Humanoid Robot Platform [19] .....	5
3.2	(a) and (b) shows lift truck operated by HRP-1 robot,based on assistance from a human operator in a motion-base system[19]. (c) and (d) shows an operator in master arm/foot system controlling the HRP-1 robot to drive a backhoe[18] .....	7
4.1	Hubo 2+ robots at Drexel University, USA .....	9
5.1	Prototype of the sensor head with Asus Xtion Pro Live and tilting Hokuyo UTM-30LX-EW, Stereo color cameras, and a PMD CamBoard nano .....	11
5.2	Hubo plus robot stepping on the vehicle in simulation and in real word [29].	12
5.3	Point cloud data from DS after distance filtering and plane segmentation ..	13
5.4	Hubo plus robot stepping on the vehicle in simulation and in real word [29].	14
5.5	Hubo plus robot stepping on the vehicle in simulation and in real word [29].	15
5.6	Ground plane and obstacle segmentation(left). The green lines are SBPL path to subgoals(yellow discs) .....	16
5.7	Hubo 2+ in the docking phase before performing ingress(left), Depth image from robot's point of view(center),rviz screen shot shows segmented vehicle's floor(blue) and edge(yellow) that guides the docking motion(right)	17
5.8	Hubo plus robot stepping on the vehicle in simulation and in real word [29].	17
6.1	Researchers involved in Driving experiments .....	18
6.2	Pedal Manipulation Phases (top) and Steering Wheel Manipulation (Bottom) .....	20
6.3	Plot made to Verify the Way Points For Steering Wheel Manipulation. ....	21

6.4	Teleoperation Interface for DRC-HUBO Driving .....	21
6.5	ID number sent to the robot and the corresponding action performed .....	22
6.6	ID number sent to the robot and the corresponding action performed .....	23
6.7	Sitting pose of the robot(left). Robot made to grasp the steering wheel at its left end(Right) .....	24
6.8	Operator Controls The Robot To Move Forward And Also To Turn 20 Degrees Clockwise Direction .....	25
6.9	DRC-Hubo teleoperated to drive in a circular pattern.....	26
7.1	Driving course for DRC [1] .....	28
7.2	Sensor head equipped with a Hokuyo LIDAR,3 FLEA-3 CCD cameras at the top,a Microstrain IMU. The sensor head is mounted on a pan and tilt unit .....	29
7.3	Joint values read from the real robot's encoder and assigned to the virtual robot in real time .....	31
7.4	Pictorial representation of Robot State Monitoring.....	31
7.5	Yellow point shows the initial position of the peg(left). Plot made by equation 6.1,which gives the way-points along the steering wheel(Right) ...	32
7.6	Images a,b,c shows a rotation of 0° to 90°. Images d, e, f shows a rotation of 90° to 180°. Images g, h, i shows a rotation of 180° to 270°. Images j, k, l shows a rotation of 270° to 360°. .....	32
7.7	Left Ankle pitch goes from initial position(35°) to final position(-5°) .....	32
7.8	Communication between the Vision Computer,the Base computer and the Robot Computer.....	33
7.9	Driving Interface for Polaris Ranger XP .....	33
7.10	DRC-Hubo manually made to sit in a drive ready pose .....	34
7.11	.....	35

7.12	DRC-Hubo driving a Polaris vehicle .....	36
7.13	A virtual model of the DRC-Hubo while it is driving .....	36
7.14	FT sensor plot: Force recorded up to 70 N(along the Z axis) at the maximum pedal press(left). Force recorded up to 50 N(along the Z axis) for a partial pressure on the pedal(right) .....	36
7.15	FT sensor plot: A force of 10 N(along the Z axis) when the foot is just placed on the pedal.....	36
7.16	Pointcloud data from the LIDAR plotted in rviz(left). RGB image stream(right). .....	36
7.17	Virtual representation of the DRC-Hubo and Sensor Head while the robot is driving .....	36



## 1. Abstract

This thesis proposes solutions for semi-autonomous driving of an Ackerman-style vehicle by a full-sized humanoid robot. A Robot Operating System based interface is developed to promote humanoid driving. The humanoid robot is also equipped with an on-board vision system which comprises of a 2D LIDAR, an inertial measurement unit and stereo cameras. Based on the visual information from the vision system, the operator specifies the operation to be performed. The operator commands the turning angle for the steering wheel and the robot takes the necessary actions to realize this task. Likewise, pressing or releasing the gas pedal is done based on the operator's request. The operator has the option of visualizing the virtual model of the robot and its work site, which facilitates command and control of the robot. Experiments are conducted on a full-sized humanoid robot DRC-Hubo, to drive a golf cart and a two-passenger utility vehicle. Previous stages of driving such as searching for the vehicle and walking towards it are also briefly discussed.

## 2. INTRODUCTION

Typhoons, hurricanes, and tsunamis have caused severe damage to human property and life over the years and at the event of such a natural disaster, secondary effects almost always occur. The explosion at the Fukushima nuclear plant during a tsunami is a very recent example. To stabilize the nuclear explosion, 580 workers were sent into an extremely hazardous environment. During this critical operation over 20 workers were badly injured and 2 of the workers died [4]. The risks involved in sending human responders to the recovery mission was catastrophic. In response to this disaster, the Defense Advanced Research Projects Agency (DARPA) set a goal to develop legged robotic systems to act as first responders for natural disaster scenarios. This event is called the DARPA Robotics Challenge which kicked off in October 2012 [1]. Fig. 2.1 shows a concept picture released by DARPA.

During future natural or accidental disasters or terrorism, a team of robotic systems will one day be sent to the disaster point to mitigate and prevent further damage. For this purpose, the robot should have the capability to transport itself to the disaster zone. Previous attempts in humanoid driving [34] [16] [18] assume and depend on an abundance of wired and wireless communications like 2-way radios, network routers, repeaters and even cell phones, between the user and robot. This is not an effective approach when viewed through the window of disaster response. The reason is that natural disasters are immediately followed by an almost total loss of communications with the outside world. Power is out, telephone services are down, and cell phone service is either non-existent or is so congested that it takes hours to get a call through. Hence during driving, the humanoid robot should have the ability to drive autonomously, move safely to a destination point, and require very little human assistance. Based on the need proposed, this thesis provides a supervised telemanip-



Figure 2.1: Humanoid systems working to reduce further disaster in a factory. This is a concept picture from DARPA.

ulation interface to allow an full-sized humanoid robot to perform driving with very minimal human intervention.



Figure 2.2: Humanoid robot DRC-Hubo seated in a driving position.

Fig. 2.2 shows a humanoid robot named DRC-Hubo placed in a seated position while manipulating the steering wheel. Humans, when working on objects of larger size, require whole body manipulation. For example, consider the actions like climbing a ladder, moving a table, or pushing a heavy object. In these instances, one coordinates their arms, hands, legs, and torso to maintain balance and interacting with the environment while performing the task. Therefore, a humanoid robot performing driving is a whole body manipulation issue. Driving in general requires the two basic operations which are pedal manipulation and steering wheel manipulation. Pedal manipulation is pressing the gas and break pedal at the appropriate time. In this case, prior to the sitting posture of the robot, the left foot alone is involved in pedal manipulation. Steering wheel manipulation is done using two different methods which will be discussed in detail in the latter part of the thesis.

In Section III, previous research on humanoid robot driving and other related work are investigated. Section IV explains the humanoid robots used in this previous research. Stages before driving like walking towards the vehicle and getting inside the vehicle is briefly looked into in Section V. Section VI and VII explain about the driving experiment with two different vehicles. Finally, Section VIII presents conclusions for this thesis.

### 3. RELATED WORK

The full-sized humanoid robot HRP-1 [14] was used to drive industrial vehicles. In [13], [20], [33], [31], and [15], considerable effort was taken in making the industrial vehicles autonomous and user friendly. Even though the process of performing teleoperation with an industrial vehicle is not impossible, the applications of such teleoperated vehicle are not numerous [16]. In [16], the HRP-1 is made to operate a lift truck, portraying that humanoid robots are not confined only to laboratories or for just entertainment. The humanoid robot was teleoperated by an operator in a remote control cockpit called a motion-base system. This teleoperation interface allows the user to experience the locomotive motion of the humanoid robot. The system comes with two exo-skeleton arms which when controlled by an operator, actuates the manipulator of the humanoid robot, forming a master-slave system. The feedback force from the humanoid robot is sent to the exo-skeleton, so the operator can have a kinaesthetic sensation of the robot. To control the open-close motion, to grasp objects, the system comes with a small gripping operation device. This indeed is a remarkable effort on the grounds of humanoid driving, but the robot's function depends entirely on the user and it requires very stable communications between the robot and the base station. Even though the robot was equipped with two on-board video cameras, no effort on sensing using vision was performed. Fig. 3.1 shows a picture of the humanoid robot HRP-1 and Fig. 3.2(a) shows the teleoperator controlling the two master arms.

[34] presents the first effort by the humanoid robot HRP to drive a back hoe in open space. In this scenario, the robot HRP-1 was equipped with protective clothing comprised of a hood, vest, sleeves, pants, and boots. The suit was seam-ventilated, drip-proof, and dust-proof. The design also makes sure that the suit does not compro-

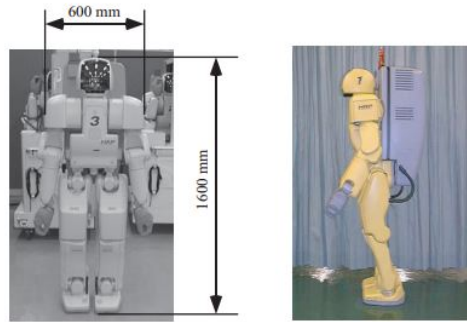


Figure 3.1: HRP-1, The Humanoid Robot Platform [19]

mise the range of motion of the robot. For teleoperation purposes, a remote control device was fabricated. It had two master arms similar to the one in [16], one master foot, two amplifier units, and one PC unit. A small pointing device was mounted on the master arm to operate the head. The master foot device consists of two tape sensors, which were attached to the ankle of the operators. The primary purpose of the master foot is to promote simultaneous control of the hands and legs of the robot. To have self-collision awareness, an on-board control system was developed and added. Stereo image data from the on-board cameras was relied upon for visual assistance. The user specified the position of the object, then the end effector moves to a position near the desired object. All these features were applied and the humanoid robot did move to a destination point and performed excavation successfully.

Even though [34] claims to use humanoid robots on non-modified industrial vehicles, there were some minor modifications made to the vehicle. The cockpit of the back hoe was partially reconstructed, floors were flattened for smooth movement of the robot, and the seat was re-modified to be a shock absorbent material for safe seating. [34], [16], and [18] are the attempts to date on humanoid robot driving (shown in Fig. 3.2).

In [32], the HRP robot performs pushing and pulling of a table through whole-

body tele-manipulation using a simple 3-axis joystick. Similarly to [34] and [16], [17] developed a teleoperation cockpit for offshore manipulation. The approach here is that the conscious operation of the robot is controlled by the user but the subconscious operations like whole body balancing and proper gait maintenance is performed autonomously. Using the Hubo 2+, [26] proposes a teleoperation framework for handling power tools like a hand held drill. [23] and [35] present work on developing teleoperation systems of the humanoid robot BHR-02 [28]. [35] focuses on developing a virtual scene of the humanoid by a combination of data such as body sensor data and the motion capture feedback. Following this work, [23] presents a teleoperation system whose architecture is client/server based using the 802.11G wireless LAN protocol. A simple joystick was used to control the head, the hand, and the whole body separately. [21] looks into the world of humanoids as an ideal response in case of emergency response.

[10] proposes an autonomous wheel robotic platform for offshore inspection and manipulation. This system was first tested in Fraunhofer IPA labs and after proper assessment, the robot was taken to an offshore gas platform. Even though it is a very decent attempt, the project was mainly focused on collision free navigation, monitoring the industrial equipment, and not much emphasis was given on manipulation of the equipment.

[8] and [9] proposes an approach for valve turning through a combination of kinesthetic teaching and a fuzzy logic system for performing autonomous valve turning in underwater environments.

The above literature shows promise of employing humanoid robots to operate vehicles. However, there are critical gaps that prevent a vertical advance in the field. In the past when a humanoid robot drives or operates a vehicle, the operator controls each joint of the robot and also relies on surplus feedback from the robot to do this.

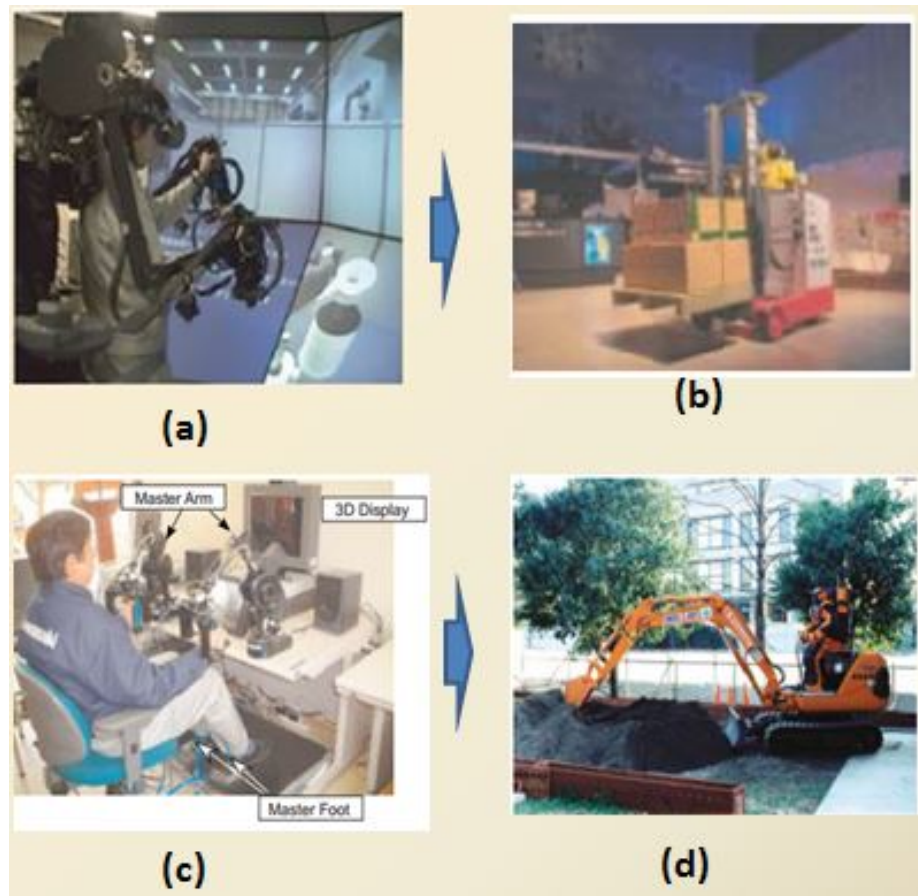


Figure 3.2: (a) and (b) shows lift truck operated by HRP-1 robot, based on assistance from a human operator in a motion-base system[19]. (c) and (d) shows an operator in master arm/foot system controlling the HRP-1 robot to drive a backhoe[18]

The master/slave relationship between the operator and the robot does not play well in disaster recovery situations where communications might be severely damaged. This thesis describes an interface which makes a humanoid robot drive a vehicle with very little assistance from the operator. Also the operator sees a virtual model of the robot and its work site in a three dimensional visual interface. The details would be explained in the latter part of the thesis.

## 4. SYSTEM OVERVIEW

### 4.1 Hubo 2+

Hubo 2+ is a humanoid robot which has a height of 130 cm and weighs 42 kg. This humanoid was developed by Dr. Jun Ho Oh, Hubo Lab, Korean Advanced Institute of Technology (KAIST) in South Korea. It has a total of 38 degrees of freedom (DoF): 6 DoF in each limb, 3 DoF in the neck, 1 DoF at the waist and 5 DoF per hand. Normal walking speed is 0.5 m/s, with a maximum speed of 1.0 m/s. It is one of the most advanced research platforms for mobile manipulation, humanoid walking and human robot interaction. Drexel University and other American universities have acquired 6 of these humanoid robots (shown in Fig. 4.1) to do collaborative research.



Figure 4.1: Hubo 2+ robots at Drexel University, USA

## 4.2 DRC-Hubo

DRC-Hubo (shown in Fig. 2.2) is also a creation from Hubo Lab at KAIST. It has a total of 32 DoF. DRC-Hubo has a more powerful 7 DoF arm and a 3-axis FT sensor with increased sensing range. The extended 6 DoF legs of 660 mm in length make them a suitable feature for driving vehicles. The hand weighs 620 grams and has 3 fingers each at a length of 11.6 cm. A single motor is responsible for actuating all 3 fingers. This feature is helpful in grasping tasks in vehicle handling and manipulating industrial objects like valves and drilling tools. Unlike Hubo 2+, DRC-Hubo was designed with a goal to perform high powered tasks like handling power tools, vehicle driving, and hose attachment to name a few. Team DRC-Hubo [2] represents the team lead by Drexel University, where DRC-Hubo was chosen to compete in the DARPA Robotics Challenge [1].

## 5. Phases before Driving

### 5.1 Detecting the Interest Points in the Utility Vehicle

Before a humanoid robot sets to drive, it has to get inside a vehicle and position itself to sit in a suitable posture, so that it can reach and manipulate the steering wheel and the pedal. This stage is called ingress. The stages of ingress was tested on a golf cart by the humanoid robot Hubo 2+ [12]. Knowledge of parts like the steering wheel, pedals and the stepping floor are necessary for motion planning for the robot, while trying to get inside the vehicle. Hence the goal was to locate and parametrize these interest points. This was discussed with more depth in my previous work [29]. To achieve this, a sensor head prototype (shown in Fig. 5.1) was developed. This was developed by Dr. Christopher Rasmussen from the University of Delaware.



Figure 5.1: Prototype of the sensor head with Asus Xtion Pro Live and tilting Hokuyo UTM-30LX-EW, Stereo color cameras, and a PMD CamBoard nano

The sensor head is equipped with an Asus Xtion Pro Live RGB-Depth camera,

a Hokuyo UTM-30LX-EW 2D lidar, a set of stereo cameras, and a CamBoard nano short range depth sensor. This unit was mounted on a tripod adjusted to have the same height as the humanoid robot Hubo 2+. With the goal being able to locate and parametrize the interest points on the Golf Kart, the tripod was made to stand around several spots near the vehicle and 3D point cloud data from the depth sensors and lidar was collected. Fig. 5.2 shows the different views from the sensor head. In PassengerMid(PM) position, the vehicle floor is in view but the steering wheel is not in view. Passenger Rear(PR) shows pedals, the floor and a partial steering wheel. Steering wheel is fully visible in position DriverSteering(DS), but the floor view is blocked by the seat. In PassengerSteering(PS), the steering wheel is in view, but the floor is not visible at all. Acquiring point cloud data (X,Y,Z values) from the Asus depth sensor was easily available through the OpenNI library. The Hokuyo lidar was made to tilt continuously in a sinusoidal pattern over a range of  $[-45^\circ, 45^\circ]$  and at maximum speed of  $10^\circ/\text{s}$ . Also the KinFu(Kinect Fusion)[25] algorithm that is part of the Point Clouds Library(PCL)[30] is considered as an other source of point cloud data. It combines multiple views from the Asus depth camera and creates a smoother surface model of the vehicle. The recognition of the vehicle parts was done using only the range based data from the Depth camera, time of flight camera and the lidar. The appearance based information was just for viewing purposes.

The point cloud data recorded by the range based sensors is manipulated to exclude the ground plane points, hence only the vehicle point cloud data remains. This was done using two different techniques. In the first technique, using a motion capture system, the height and tilt angle of the sensor head with respect to the ground plane was reported. This is used to locate ground points ( $|z| \leq 0.1$  m). In the second technique, RANSAC robust plane-fitting with an inlier threshold distance of 0.01 m followed by least squares refinement is applied to the rough ground points to obtain

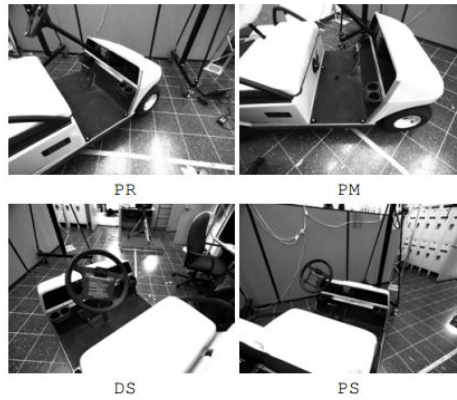


Figure 5.2: Hubo plus robot stepping on the vehicle in simulation and in real word [29].

the final ground plane. The resultant plane is used to rectify the original sensor point cloud and remove ground points with a threshold of 0.05 m. Also points 2 m away are neglected. Fig. 5.3 shows the resultant point cloud data. With the non-vehicle points trimmed away, the vehicle's point clouds are further worked upon to recognize steering wheel and the floor.

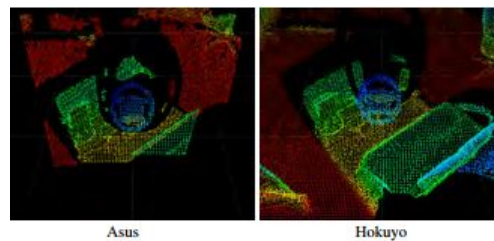


Figure 5.3: Point cloud data from DS after distance filtering and plane segmentation

### 5.1.1 Locating the Floor

The floor of the vehicle, where the robot has to step on to, is a rectangular object parallel to the ground plane. Applying RANSAC (Random Sample Consensus) algorithm to the whole vehicle’s point cloud will also yield the seat or the hood planes. However, we have prior knowledge that the floor plane must be at a reachable height. So specifications from a set of exemplar vehicles like the Cushman Hauler and Kawasaki Mule were considered to get the estimate of the floor height (which is  $z_{floor} \in [0.15, 0.40]$ ). Considering the registered sensor point cloud in this window, yields a nominal floor slice upon which RANSAC horizontal plane fit is applied, where the normal must be within 5 deg of vertical. Fig. 5.4 shows floor plane inliers for each sensor view  $F_s^*$  in green and outlier points are in red. Extracting the cluster of inliers belonging to the floor region itself can be formulated as a rectangle finding problem. The floor’s rectangle are assumed to align with those of the vehicle and the width is approximately the same as the vehicle and its center is on the vehicle centerline. Hence only 2 free variables are to be determined, which are floor’s backward/forward position ( $R_{floor} : (x_{floor}, l_{floor})$ ) and the distance between the seat and the dashboard. Applying reasonable bounds on these variables and running a particle filter (for 10 iterations) with the likelihood function  $P_{floor}(R) = (N_{in} - N_{out})/A$ .  $N_{in}$  is the number of floor plane inliers in  $R$  and  $N_{out}$  is the number of outliers in the rectangle,  $A$  is the rectangle’s area. The blue lines in Fig. 5.4 indicates the estimated floor rectangles. The rectangular region is detected well, when the whole floor region is visible. Features like pedals, drink holders and steering wheel are detectable as outlier points and present inside the floor rectangle. This would be useful to the motion planner.

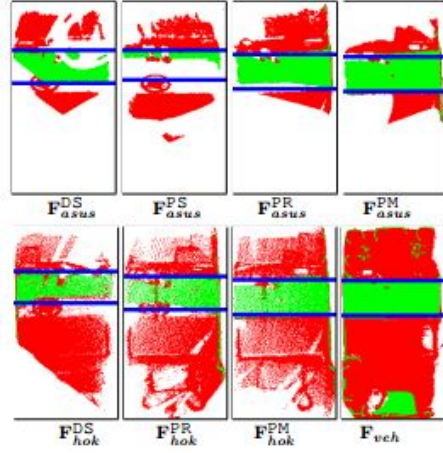


Figure 5.4: Hubo plus robot stepping on the vehicle in simulation and in real word [29].

### 5.1.2 Locating the Steering Wheel

A steering wheel is basically a circle in 3D space with a specific orientation. Based on automotive standards, there are tight bounds on the possible radius  $r$  and the orientation of the steering wheel is considered to be in the range of  $\phi \in [20^\circ, 70^\circ]$ . Hence the approach is to interpret a discrete steering wheel pose and size hypothesis in terms of an axis-aligned bounding rectangle  $R_{sw}$  in a registered sensor heightmap  $H_s^*$ . The center of the rectangle is  $\mathbf{x}_{sw}, \mathbf{y}_{sw}$ , the width would be  $2r_{sw}$  and the length is  $2r_{sw} \cos \phi$ . The criteria was that the points on the ellipse(found within this bounding rectangle)should be in contrast with the points lying outside the bounding rectangle. Hence we start with  $N$  discrete points, it is then split into  $N_{in}$ (inside points) and  $N_{out}$ (outside points). The probability of the associated rectangle is then  $P_{sw}(\mathbf{R}) = (N_{in} - N_{out})/N$ . Running a particle filter for 200 iterations over different rectangles to optimize  $P_{sw}$ . If the likelihood of the best rectangle is less than 0.5, it is assumed that the steering wheel is not found. Fig. 5.5 shows the result of this search.

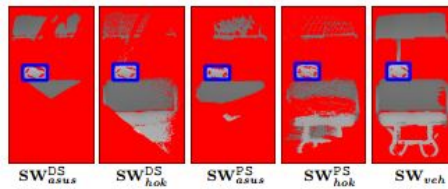


Figure 5.5: Hubo plus robot stepping on the vehicle in simulation and in real word [29].

## 5.2 Approaching the Vehicle

Before a humanoid robot sets to drive a vehicle, there is a requirement to locate the vehicle in a cluttered scene and walk towards it. In section 5.1.1, the floor of a golf cart was located. This is considered as the goal point for the robot. Motion goals during this phase are specified in an odometric frame with its origin at the robot's initial position. In order to reach this goal, there is a need to localize the robot. The plan is to update odometry as the robot walks. Visual odometry is the solution here. The details of the visual odometry approach will not be discussed here. The sensor head seen in figure 5.1 is modified to accommodate two RGB-D cameras. Two Asus Xtion Pro Live RGB-D cameras are mounted with a  $45^\circ$  pitch difference between them. Depth and color images were captured from each sensor at  $320 \times 240$  resolution at 30 fps. This sensor head is mounted at a fixed pitch angle of  $30^\circ$  below horizontal. The total vertical field of view of the camera is about  $80^\circ$ . The horizontal field of view is  $60^\circ$ . For a wider view, the robot pans its waist joint as seen in figure 5.7(left).

The humanoid robot Hubo 2+ walking motion is not planned by the foot step planner as in [11], but through modal directives such as "walk forward", "stop" and "turn in place". The robot's step length are constant 5 cm each. Hence a search based planner built on straight and turn in place motion primitives [27], [22] which relies on costmap generated from the obstacles found after ground plane extraction.

Figure 5.6 shows the outcome of a search based planner. The gray colored areas are the obstacles and the green lines would be the collision free path.

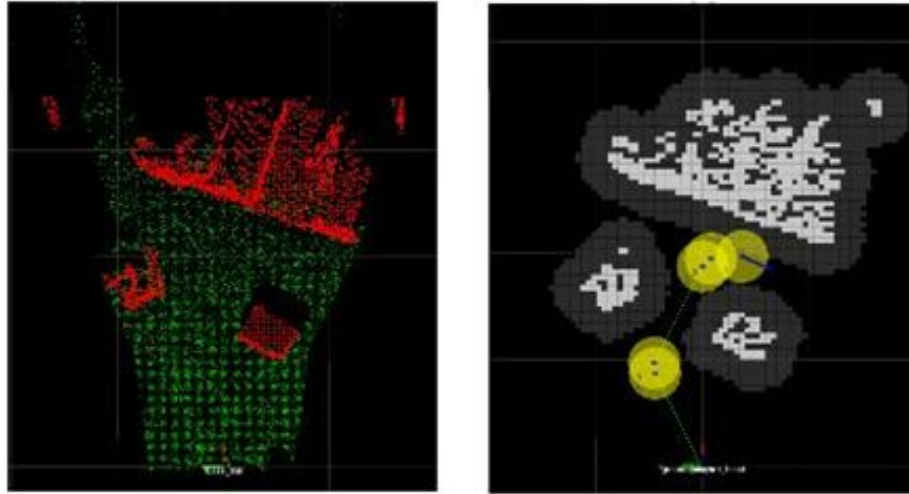


Figure 5.6: Ground plane and obstacle segmentation(left). The green lines are SBPL path to subgoals(yellow discs)

### 5.2.1 Docking Phase

After the robot reaches near the vehicle's floor, the next step is to perform ingress, which is to step inside the vehicle. In the section 5.1 the coordinate system was based on the robot, but in this phase it is switched to vehicle based coordinate system. The origin is set to the forward end of the vehicle's floor. If the vehicle's floor can be visualized and tracked, the error could be directly measured between the robot's pose and the vehicle floor's pose  $(x,y,\theta)$ , where  $\theta$  is the angle between the robot heading and the base floor's line segment. Through simulation and experiments, it is found that ideal position to do ingress is  $0.1 \text{ m} \times 0.1 \text{ m} \times 5^\circ$ .

If the robot is already in the ideal pose in the docking phase, ingress could be

performed directly or else the robot has to reposition itself to get into that ideal pose. This is done by directly tracking the golf cart's floor(as shown in figure 5.7(right)) and perform position based visual servoing on it, to reduce the error. Similar to approach phase, the robot is allowed to step forward and turn in place, but the step lengths are shortened to 2.5 cm. Once this phase is successfully completed, the robot performs ingress as shown in figure 5.8. The details of the ingress phase is beyond the scope of this thesis.



Figure 5.7: Hubo 2+ in the docking phase before performing ingress(left), Depth image from robot's point of view(center),rviz screen shot shows segmented vehicle's floor(blue) and edge(yellow) that guides the docking motion(right)

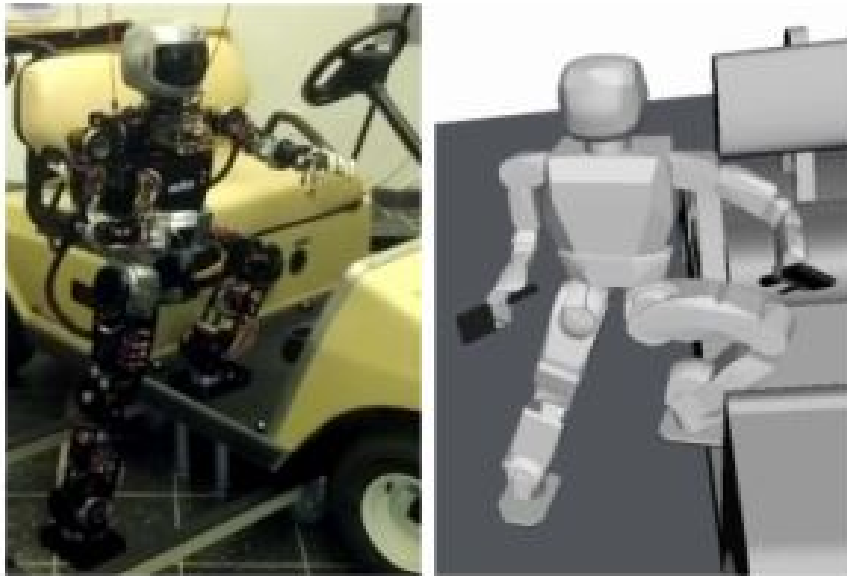


Figure 5.8: Hubo plus robot stepping on the vehicle in simulation and in real word [29].

## 6. Driving a golf cart with a humanoid robot

Humanoid driving experiments involves the work from other researchers as well. The sensor head was developed by Dr. Christopher Rasmussen. The whole body IK solver used in manipulating the vehicles was developed by Dr. Inhyeok Kim. The telemanipulation interface developed involves their work too. Fig. 6.1 shows a figurative picture of the fellow researchers involved.

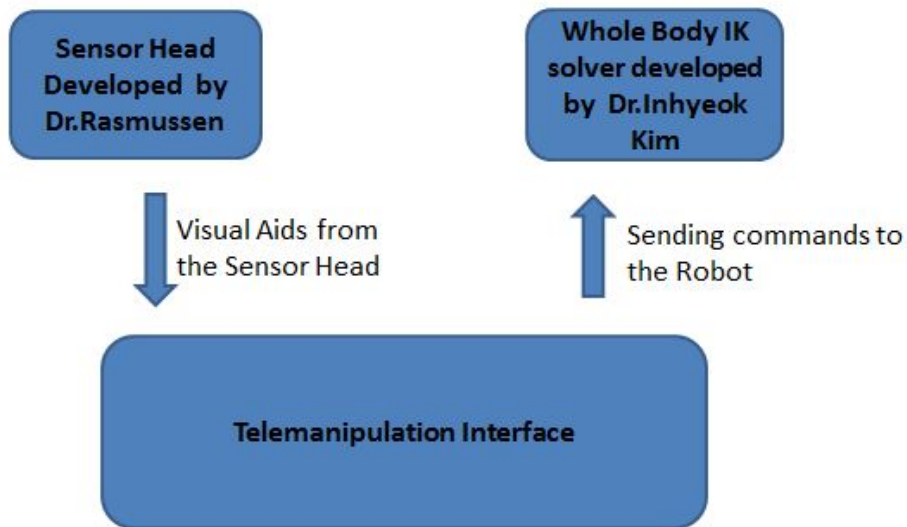


Figure 6.1: Researchers involved in Driving experiments

The humanoid robot discussed in Section 5.6 was made to drive two kinds of vehicles: a Polaris Ranger XP 500 and a golf cart. The difference in inner dimensions of these vehicles significantly affects the two parameters:

- Sitting posture of the robot.

- Way of manipulating the pedals and the steering wheel.

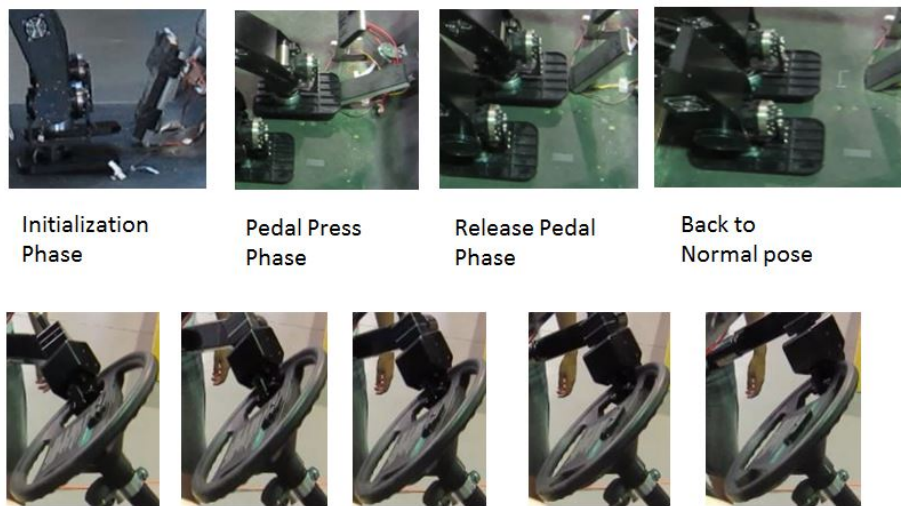
Features like the sensitivity of the gas pedal and the presence/absence of power steering on the vehicle make a major difference while manipulating the vehicle. The Polaris ranger XP has a power steering feature whereas the golf cart does not have that feature. This makes the manipulation of the steering wheel in the Polaris model much easier.

### 6.1 Manipulating the Steering Wheel and the Pedal in a golf cart

The steering wheel's radius and its orientation along the Y axis is measured manually. These parameters are fed into Equation 6.1 and a plot (as shown in Fig. 6.3) is made in 3D space in MATLAB. These are basically way points for the end effector. The robot's left hand is made to grab at a suitable point on the steering wheel manually. Based on given angle of turn (say  $10^\circ$ ) and the current position of the hand (say at  $0^\circ$ ), the corresponding end effector positions X,Y,Z are produced from  $0^\circ$  to  $10^\circ$  with an offset of  $0.01^\circ$ . That is, the Cartesian coordinates produced by Equation 6.1 is passed to an on-line whole body IK solver. The whole body IK solver gives out the corresponding joint values (for the left end effector) to reach the destination Cartesian coordinate, hence rotating the steering wheel to a desired degree. The steering wheel of the utility vehicle does not have a power steering feature. Tests proved that rotating the steering wheel in a range of  $40^\circ$  or  $-40^\circ$  resulted in over-heating and breakage of the shoulder joints. Hence the safe limit of rotation would be  $30^\circ$  or  $-30^\circ$ .

$$\begin{pmatrix} X \\ Y \\ Z \end{pmatrix} = \begin{pmatrix} C\_X \\ C\_Y \\ C\_Z \end{pmatrix} + \begin{pmatrix} 0 \\ 1 \\ 0 \end{pmatrix} \left( r * \cos(\theta) \right) + \begin{pmatrix} \sin(\phi) \\ 0 \\ \cos(\phi) \end{pmatrix} \left( r * \sin(\theta) \right) \quad (6.1)$$

- $\theta$ - Desired turn for the steering wheel.
- $\phi$  - Orientation of the steering wheel along the Y axis.
- X,Y,Z - Destination coordinate for the desired turn of the steering wheel.
- C\_X,C\_Y,C\_Z- Centre of the steering wheel



DRC HUBO Completing a 30 Degree Turn On the Steering Wheel

Figure 6.2: Pedal Manipulation Phases (top) and Steering Wheel Manipulation (Bottom)

Manipulating the pedal is done using the left foot of the robot. Similar to manipulation of steering wheel, the Cartesian coordinates for the left foot is given to on-line IK solver, which sends out the joint values to complete the motion. In pedal manipulation only the gas pedal is being manipulated here. The reason is that after the robot finishes driving in DARPA Robotics Challenge, it has to get outside and walk to a destination point (this phase is called egress). Hence the robot is made to sit in

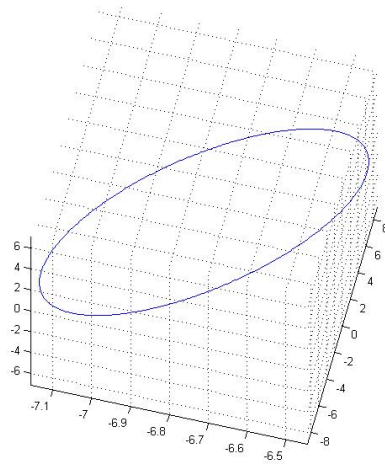


Figure 6.3: Plot made to Verify the Way Points For Steering Wheel Manipulation.

a posture as shown in Fig. 2.2. In this seated position the left foot is in front of the gas pedal. Pressing the gas pedal happens through the following phases:

- Initialization Phase- Left foot is lifted 2 cm(along the Y axis) above the vehicle's floor.
- Pedal press Phase- The gas pedal is pressed at a constant force, by moving the foot along the X axis.
- Release Pedal Phase- The foot releases the pedal and goes to the initial phase.
- Back to normal pose- The foot comes back to initial normal sit posture.

Fig. 6.2 shows the steering wheel and pedal manipulation done on the golf cart.

## 6.2 Driving Interface for a Golf cart

Fig. 6.4 shows the interface developed for driving experiment with a golf cart. An X-BOX controller communicates with a receiver through RF 2.4 GHz protocol.

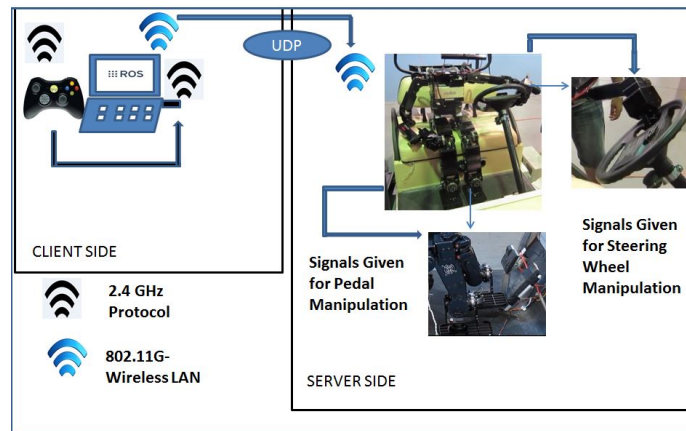


Figure 6.4: Teleoperation Interface for DRC-HUBO Driving

The receiver which has a universal serial bus (USB) is connected to a computer which is running on LINUX. On this computer, a ROS [24] node listens to the joystick messages and in-turn communicates with the on-board computer of the humanoid robot through 802.11G wireless LAN based on UDP(User Datagram Protocol)communication. Basically on each button press on the x-box controller, a unique number is sent to the humanoid robot as an UDP packet. Fig. 6.5 shows a table of numbers sent and the corresponding action performed. The symbol "ROS" seen



Button	ID sent	Relevant action
X	2	Steer 30 degrees counter clockwise.
B	3	Steer 30 degrees clockwise.
A	4	Release foot from the pedal.
Y	5	Press pedal

Figure 6.5: ID number sent to the robot and the corresponding action performed

in the Fig. 6.4 on the base computer (left side) denotes that the programs sending the commands are ROS nodes. Fig. 6.6 shows a detailed picture of the ROS nodes communicating with the robot's on-board computer. A ROS node is a process which performs computation. A ROS topic is a median through ROS nodes exchange messages [24]. In the Fig. 6.6, a node named "Joy" sends out messages to the named topic "joy". The node named "Teleop\_Drive" subscribes to this topic. The computer on the robot listens for UDP packets for every 200 ms.

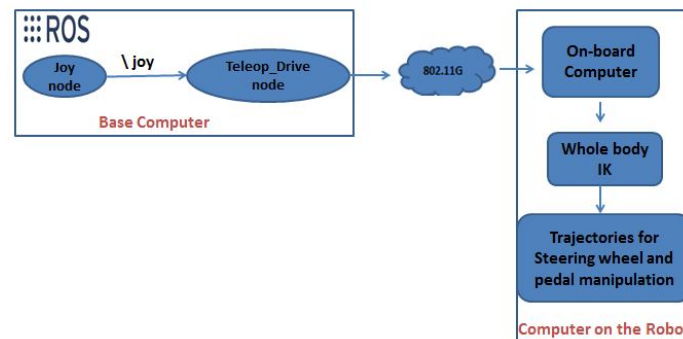


Figure 6.6: ID number sent to the robot and the corresponding action performed

### 6.3 Driving Experiment-1

The robot is brought to the pose as shown in Fig. 6.7 (left). Then the robot is made to sit in the golf cart by user's assistance. The left hand of the robot is made to grasp the left end of the steering wheel, this is shown in Fig. 6.7(right). In the coordinate system, this grasp point is considered as the origin. In Fig. 6.8 user sends the commands using the joystick being held in hand. The user initializes the left foot of the robot, this is called the Initialization phase (see Fig. 6.2). Then the press pedal phase command is sent. This makes the golfcart move forward. In the Fig.

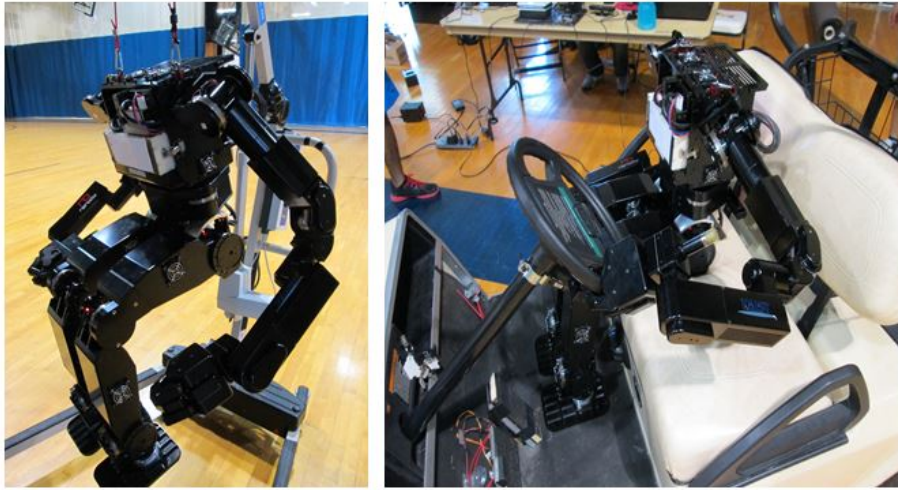


Figure 6.7: Sitting pose of the robot(left). Robot made to grasp the steering wheel at its left end(Right)

6.8, the robot drives forward and makes a 20° clockwise turn on the steering wheel. Then the release pedal phase is sent by the user, which makes the vehicle come to a halt. The time taken to see the actual manipulation on the steering wheel or the gas pedal is not more than 2 seconds. In Fig. 6.9 the robot rotates the steering wheel 30



Figure 6.8: Operator Controls The Robot To Move Forward And Also To Turn 20 Degrees Clockwise Direction

degrees counter clockwise, holding the steering wheel in this position the pedal press command is given, which makes the golf cart move in a circular pattern.



Figure 6.9: DRC-Hubo teleoperated to drive in a circular pattern

## 7. Driving with Polaris Ranger XP

### 7.1 Driving event in DRC-2013

The vehicle used for the driving event in DRC(2013) is Polaris Ranger XP 900. In the event, the robot is made to sit inside the vehicle manually. The robot is set in a way, so it can have access to the gas pedal and the steering wheel. Once the robot is set, the operator will no longer have access to the robot. The next step is to command the robot to drive the course (shown in the figure below) without colliding into the obstacles. The total length of the course is 0.0473 miles and it has 6 barriers angled at  $45^\circ$ . In order to drive this course successfully the following features are

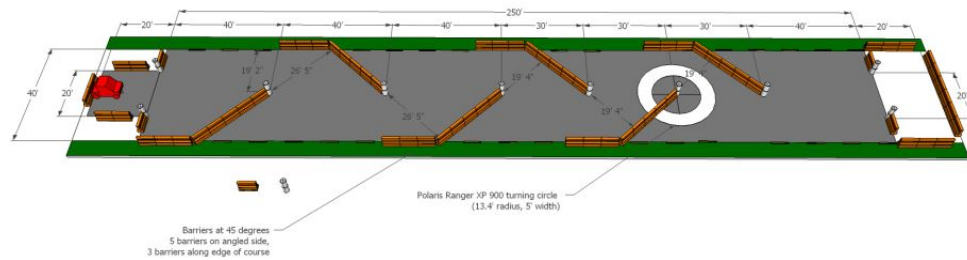


Figure 7.1: Driving course for DRC [1]

needed:

- The operator should be able to see through the robot's on board camera while telemanipulating the robot.
- The operator does not interfere with the robot while driving, so there should be a means to monitor the robot.

- The robot should have the capacity to make massive turns on steering wheel to avoid the obstacles.

Based on the needs, extra features were added to the driving interface discussed in section 6.2. Each of these features will be discussed in the following sections.

## 7.2 Sensor Head

A clear view of what the robot is seeing and also the distance of the obstacles from the vehicle is very important for the operator to perform the driving safely and also to complete the course. Considering this need, the robot is equipped with a sensor-head similar to the unit discussed in section 5.2.1 but with some alterations considering the nature of the driving event. The robot has to drive the vehicle outside in the presence of sunlight. The 2 RGB-D sensor Asus Xtion Pro Live used in the section 5.2.1 cannot be used for this event, as they cannot function in the sunlight. The sensor head for driving (shown in figure 7.2) is equipped with Hokuyo UTM-30LX-EW a 2D LIDAR, Microstrain 3DM-GX3-45 an IMU (equipped with GPS) and 3 FLEA3 cameras. The Hokuyo LIDAR has range of 30 m and has a sweep of  $270^\circ$ . Before the robot sets to drive, there is a requirement to scan the scene with the LIDAR, so the operator could see the proximity of obstacles from the vehicle. This is done by tilting the Hokuyo LIDAR between  $60^\circ$  and  $-40^\circ$ , this scan could be visualized in ROS rviz. 2 MX-106 dynamixels are mounted on the sensor head, one for pitch motion and another for yaw. In section 5.2.1, the sensor head was fixed, so the whole robot has to move in order to monitor the scene. But in this case, just the sensor head has to be controlled to monitor the scene.



Figure 7.2: Sensor head equipped with a Hokuyo LIDAR,3 FLEA-3 CCD cameras at the top,a Microstrain IMU. The sensor head is mounted on a pan and tilt unit

### 7.3 Monitoring the state of the humanoid robot

In figure 6.8, the operator moves along with the golfcart, while the robot drives it. Basically the operator is visually confirming the commands, he sent to robot's computer. But this cannot happen in DRC, as the operator is not allowed to monitor the robot in person while it drives. But providing a complete scene of the robot and its work site will increase the efficiency of teleoperation [35]. Hence an URDF(Universal Robot Description Format) model of the humanoid robot is used to imitate the current state of the real robot and it is visualized in ROS rviz.

For every 300 ms, the joint values of the robot is sent as UDP packets to the operator's computer. Then these values are assigned to the corresponding joints of the URDF model. The 3-axis FT(Force Torque) sensor from the robot's hand and foot is also sent as UDP packets to the operator's computer. In Figure 7.3 the joint values from the real robot is assigned to the corresponding joints in the URDF model. This can help the operator have a better sense of the robot's current state while driving. This module is used in the DRC(2013)[1] by Team DRC-Hubo on the events Driving, Hose Attachment and Rough Terrain Walking. Fig. 7.4 shows the

pictorial representation of the module.

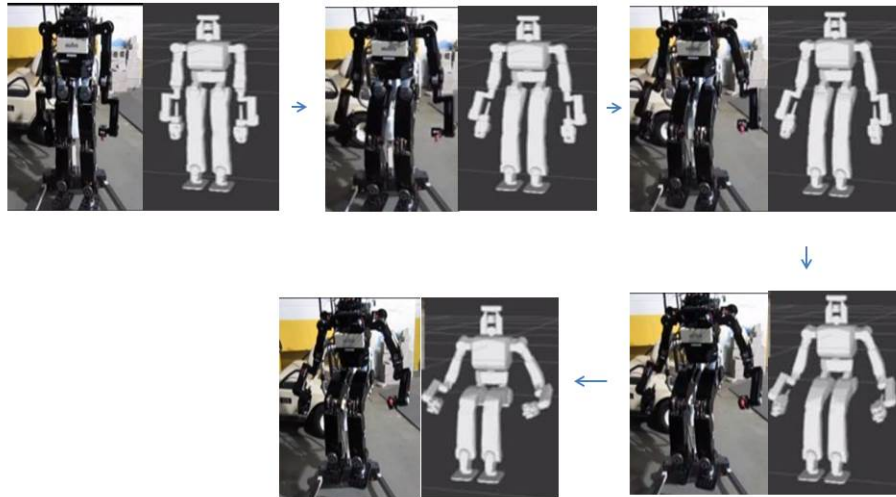


Figure 7.3: Joint values read from the real robot's encoder and assigned to the virtual robot in real time

#### 7.4 Manipulating the Steering Wheel and the Pedal in the Polaris Ranger XP

In section 6.1, the left end of the steering wheel was grasped and rotated along its circumference. Here instead of the grasping the steering wheel, the peg was used to insert into it and then dragged to the destination location along the circumference of the wheel. In Fig. 7.5, the yellow point shows the initial position of the steering wheel and the blue triangle shows the region within which the peg moves to drag the steering wheel to the destination position. The radius of the steering wheel which is

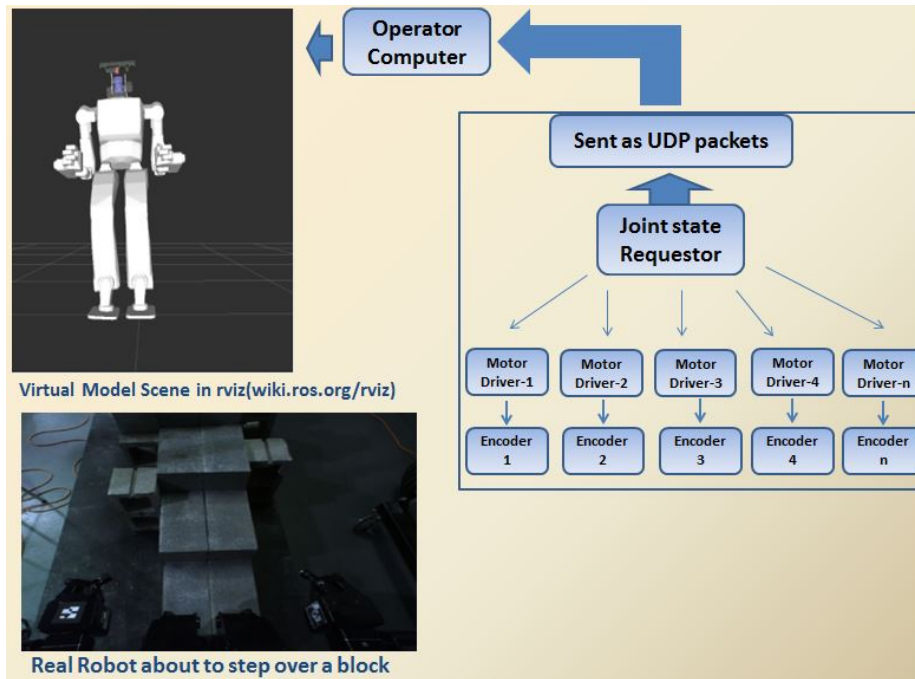


Figure 7.4: Pictorial representation of Robot State Monitoring

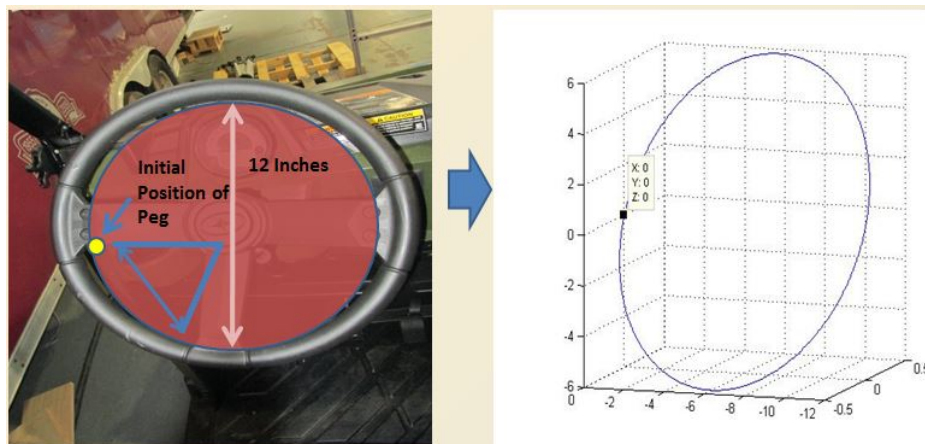


Figure 7.5: Yellow point shows the initial position of the peg(left). Plot made by equation 6.1,which gives the way-points along the steering wheel(Right)

6 inches and inclination along the Y axis, which is  $59^\circ$  is given to the equation 6.1. For  $\theta = 360^\circ$  in equation 6.1, an exact plot of the steering wheel is made. In the Fig. 7.6, the steering wheel is rotated from  $0^\circ$  to  $360^\circ$ . For manipulating the gas

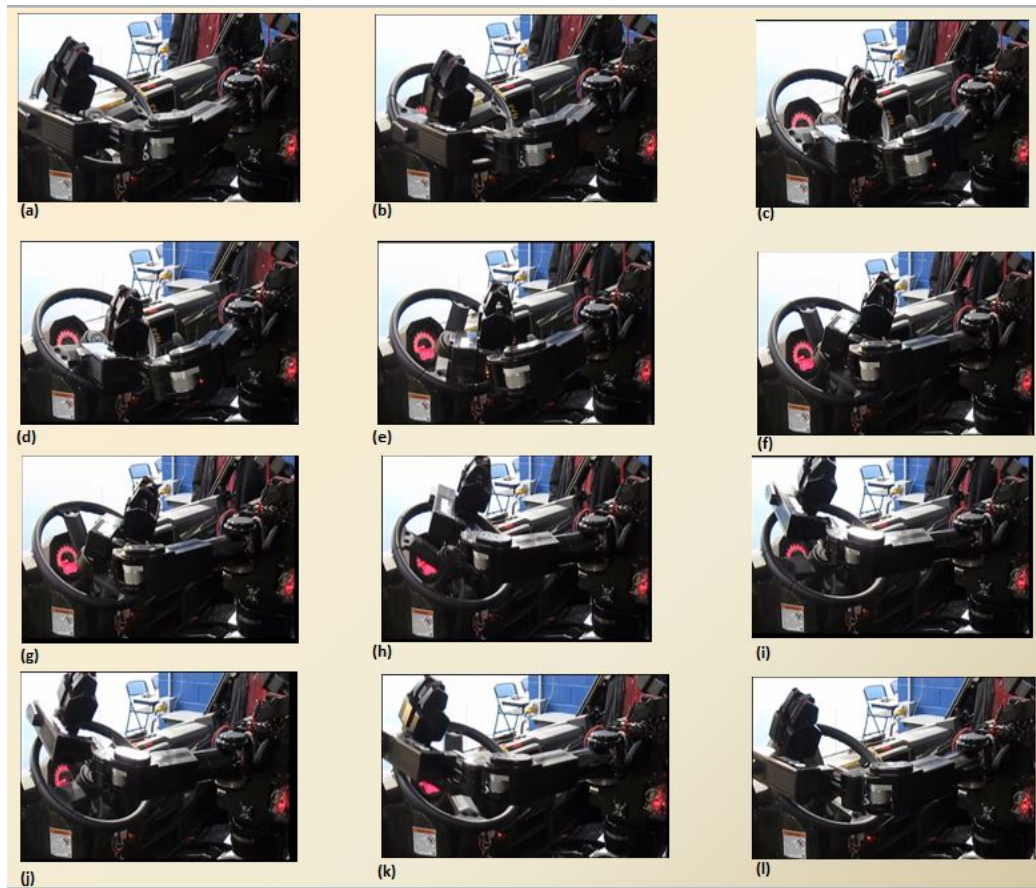


Figure 7.6: Images a,b,c shows a rotation of  $0^\circ$  to  $90^\circ$ . Images d, e, f shows a rotation of  $90^\circ$  to  $180^\circ$ . Images g, h, i shows a rotation of  $180^\circ$  to  $270^\circ$ . Images j, k, l shows a rotation of  $270^\circ$  to  $360^\circ$ .

pedal, the left foot of the robot is placed parallel to the plane of the gas pedal(as shown in Fig. 7.7). In Fig. 7.7, the left ankle pitch joint is at  $35^\circ$  and after pressing the pedal, it is at  $-5^\circ$ . Hence during the pedal press phase, when the left ankle pitch is at  $35^\circ$ , there would be no motion in the vehicle, this is the initial stage of the gas pedal manipulation. In the second stage, the gas pedal would be pressed until the left ankle pitch reaches to  $-5^\circ$ . This is called the final stage, where the vehicle(Polaris ranger) moves at 2 miles/hr.



Figure 7.7: Left Ankle pitch goes from initial position( $35^\circ$ ) to final position( $-5^\circ$ )

## 7.5 Driving interface for the Polaris ranger XP

The robot's on-board computer contains an ATOM processor 1.6 GHZ and a RAM of 2 GByte. While this is enough for functioning of the humanoid robot, it does not have capacity to process the data from the ladars and depth sensors. Hence a back pack was created on the robot. A computer with Intel i5 processor is placed in the back pack. This would called as the "vision computer". Fig. 7.8 shows the roles of

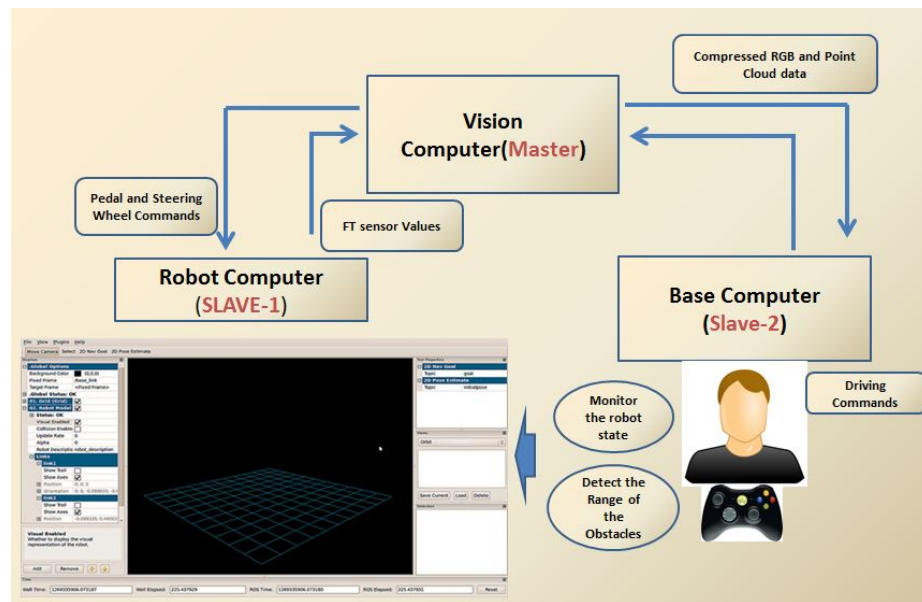


Figure 7.8: Communication between the Vision Computer, the Base computer and the Robot Computer

the vision computer:

- Receive joint values and FT sensor values from the robot's computer
- Send steering commands on operator's request to the robot's computer
- Send pedal press/release commands on operator's request to the robot's computer
- Allows the operator to control the movement of the sensor head
- Streaming compressed RGB image and point cloud data to the base computer to be visualized in rviz[6]

Fig. 7.9 shows the driving interface used for the polaris vehicle. Theora based compression[7] and "Image\_transport" package[5] in ROS[24] are the two main factors involved in compressed streaming(based on TCP) of the image data and the point cloud data from the stereo camera and LIDAR respectively.

## 7.6 Driving Experiment-1

The following points explains on setting up the robot:

- The robot is brought to a seating pose.
- After this, it is placed inside the utility vehicle.
- Then the peg on the left hand of the robot is placed in the triangular region shown in Fig. 7.5.
- The right hand is manually made to grasp at a handle of the vehicle.
- Fig. 7.10 shows the robot seated inside the utility vehicle and also the position of the left hand.

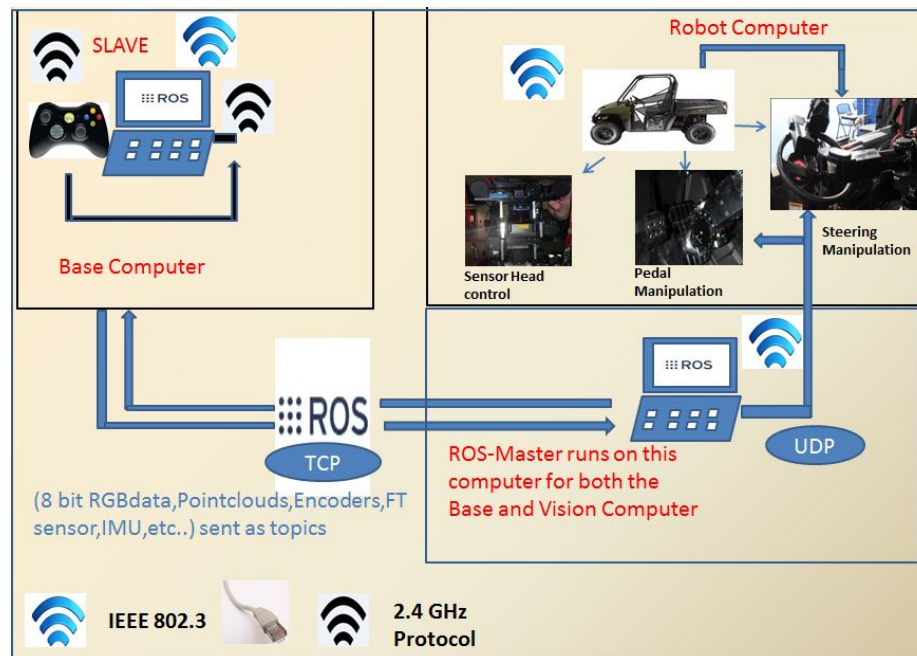


Figure 7.9: Driving Interface for Polaris Ranger XP

- The sensor head described in section 7.2 is attached to the robot's torso and vision computer is placed on the back pack of the robot.
- The FLEA camera, the IMU and the pitch-yaw unit are connected to the vision computer.
- An ethernet cable from the Hokuyo LIDAR, the vision computer and the robot computer is connected to an ethernet hub, this assures that these modules are on the same network.
- A separate ethernet cable connected to this ethernet hub is connected to the base computer. This assures data exchange between the robot computer, vision computer and the base computer.

The gear of the utility vehicle is set on a low gear. The test was conducted in a parking lot with pillars as obstacles. In Fig. 7.11 and 7.12, the robot drives along the parking



Figure 7.10: DRC-Hubo manually made to sit in a drive ready pose

lot avoiding collision with the pillars. While driving, the operator also keeps note of the virtual robot in rviz[6]. The steering and pedal manipulation brings movement on the left hand and foot respectively. This movement could be seen on the virtual robot real time, which gives a confirmation to the operator, that the commanded task is being done. A plot of the FT sensor data on the left foot(which presses the gas pedal)is being made. In Fig 7.14, when the left ankle pitch is at  $-5^\circ$ , that is when pressing the pedal at the legs maximum limit. A force of 70 N is recorded and this results in 2 miles per hour motion on the vehicle. When the foot comes back to its normal pose, which is at  $35^\circ$  a force of 10 N is recorded.

As discussed in section 7.5, the point cloud data and the RGB image frames from the laser range finder and FLEA camera is accessed by the vision computer. The data is compressed and sent over an ethernet cable to the base computer based on TCP/IP protocol. Fig. 7.16 shows the point cloud data plotted in rviz[6](left) and the video

streaming from the FLEA camera(right). A ROS [24] package named "Hokuyo\_node" [3] takes care of the plotting of the point cloud data. An Universal Robot Description Format(URDF) model of the sensor head was created by Dr. Christopher Rasmussen, University of Delaware. This model is made to mimic the encoder values of the dynamixels on the actual sensor head, but this work is beyond the scope of this thesis. Fig. 7.17 shows the virtual model of the sensor head and the robot while driving(left).

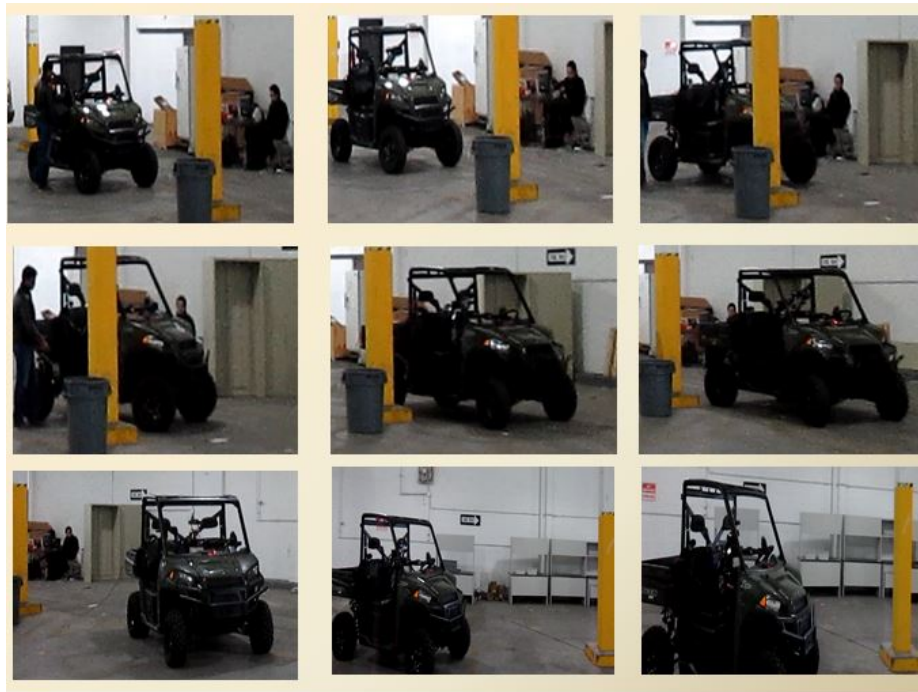


Figure 7.11

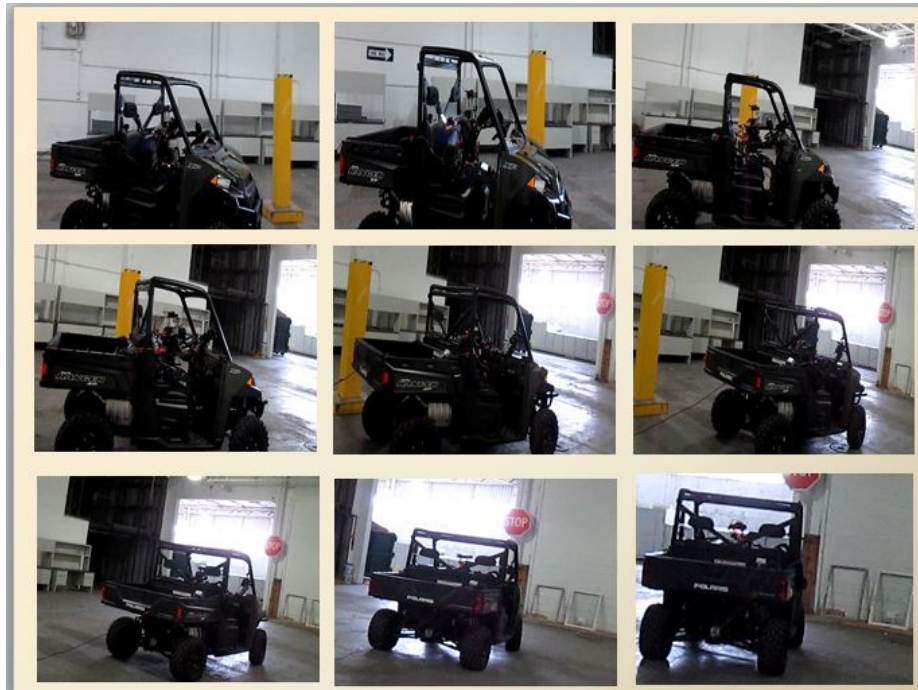


Figure 7.12: DRC-Hubo driving a Polaris vehicle

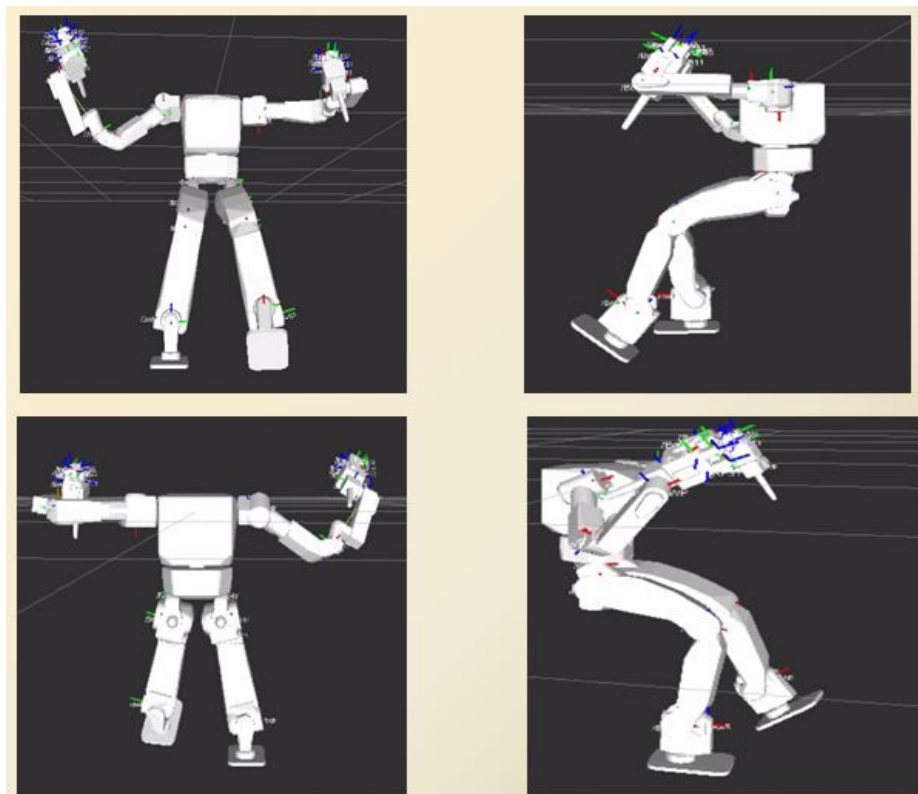


Figure 7.13: A virtual model of the DRC-Hubo while it is driving

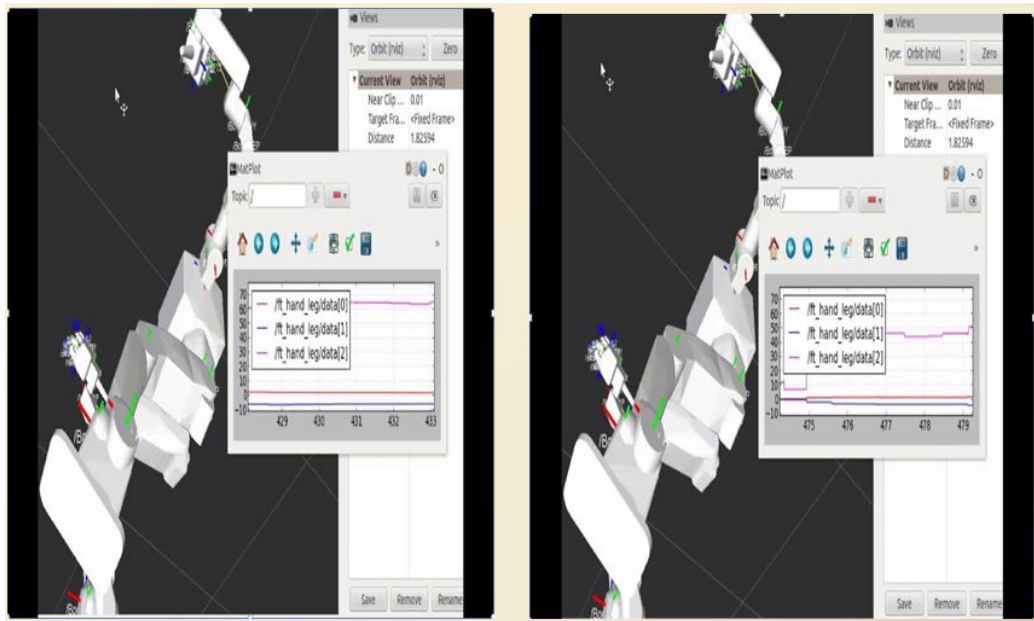


Figure 7.14: FT sensor plot: Force recorded up to 70 N(along the Z axis) at the maximum pedal press(left). Force recorded up to 50 N(along the Z axis) for a partial pressure on the pedal(right)

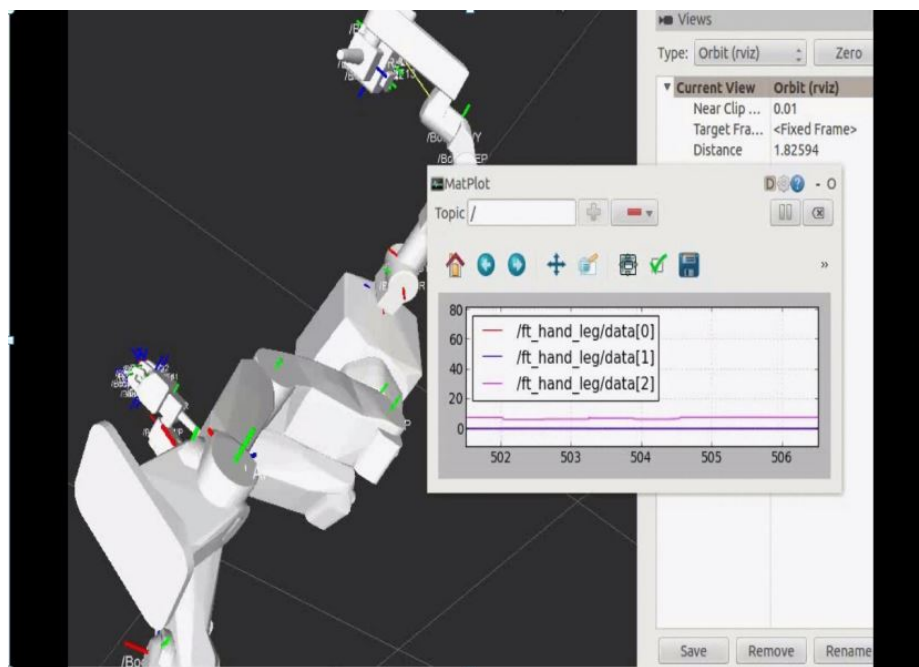


Figure 7.15: FT sensor plot: A force of 10 N(along the Z axis) when the foot is just placed on the pedal

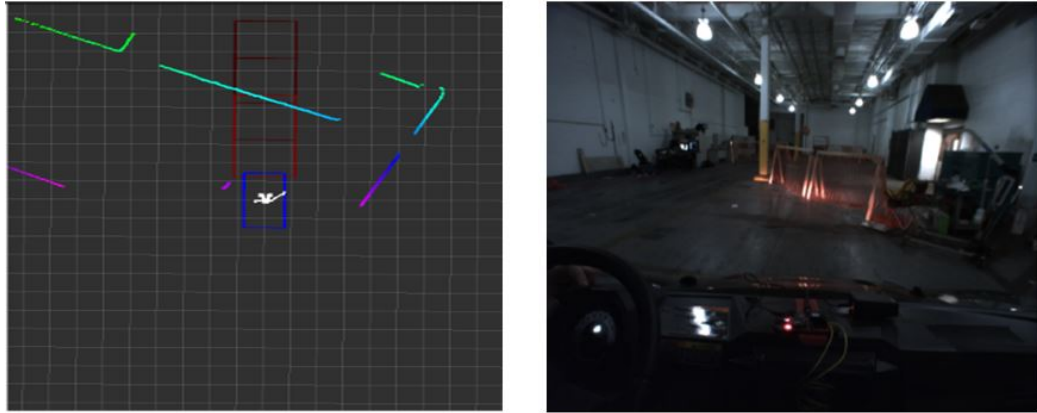


Figure 7.16: Pointcloud data from the LIDAR plotted in rviz(left). RGB image stream(right).

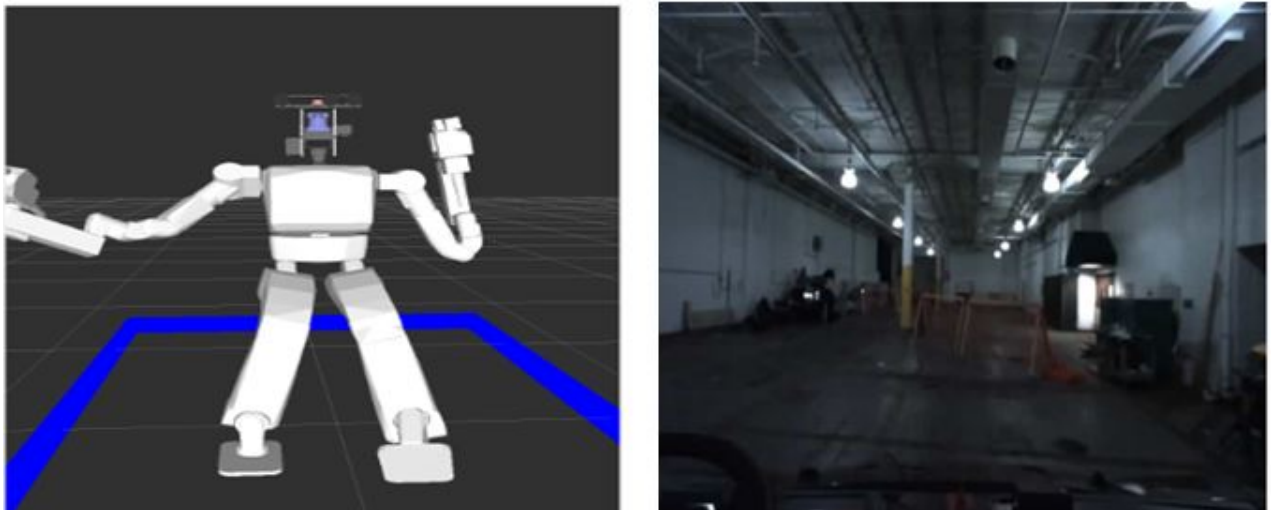


Figure 7.17: Virtual representation of the DRC-Hubo and Sensor Head while the robot is driving

## 8. Conclusion

Initially, solutions for detecting interest points on a golf cart to perform humanoid ingress was explained. After the interest points were detected the humanoid robot was made to walk towards the goal(vehicle's floor) in a cluttered scene. A supervised telemanipulation interface was developed for humanoid driving. This interface was successfully tested on 2 kinds of Ackerman-style vehicles. Gear manipulation and break pedal manipulation will be considered in the future work. Also the gas pedal and steering wheel manipulation does not happen in the same time, due to this there is a considerable delay during driving. Hence performing steering and pedal manipulation simultaneously would be considered in the future effort. In section 5.1 an Search Based planners was used to direct the robot to the goal position. This planner could be used to plan a collision free path for the vehicle based on the sensory feedback from the robot's sensor head, hence leading to autonomous driving.

## Bibliography

- [1] Darpa” darpa robotics challenge website” available at <http://darparoboticschallenge.org> accessed december,2012.
- [2] <http://dasl.mem.drexel.edu/drc/>.
- [3] [http://wiki.ros.org/hokuyo\\_node](http://wiki.ros.org/hokuyo_node).
- [4] ”the asahi shimbun,availaible at [https://ajw.asahi.com/article/0311disaster/life\\_and\\_death/AJ201103193106](https://ajw.asahi.com/article/0311disaster/life_and_death/AJ201103193106)”.
- [5] [wiki.ros.org/image\\_transport](http://wiki.ros.org/image_transport).
- [6] [wiki.ros.org/rviz](http://wiki.ros.org/rviz).
- [7] [www.theora.org](http://www.theora.org).
- [8] A. Ajoudani P. Kormushev M. Carreras A. Carrera, S. R. Ahmadzadeh and D. G. Caldwell. ”towards autonomous robotic valve turning”. In *Cybernetics and Information Technologies. Issue 3*, volume 12, page 1726, 2013.
- [9] Seyed Reza Ahmadzadeh, Petar Kormushev, and Darwin G. Caldwell. ”autonomous robotic valve turning: A hierarchical learning approach”. In *Robotics and Automation (ICRA), 2013 IEEE International Conference on*, pages 4614–4619. IEEE, 2013.
- [10] M. Bengel, K. Pfeiffer, B. Graf, A. Bubeck, and A. Verl. ”mobile robots for offshore inspection and manipulation”. In *Intelligent Robots and Systems, 2009. IROS 2009. IEEE/RSJ International Conference on*, pages 3317–3322, 2009.
- [11] J. Chestnutt, Y. Takaoka, K. Suga, K. Nishiwaki, J. Kuffner, and S. Kagami. ”biped navigation in rough environments using on-board sensing”. In *Intelligent Robots and Systems, 2009. IROS 2009. IEEE/RSJ International Conference on*, pages 3543–3548, 2009.
- [12] R. Ellenberg, R. Sherbert, P.Y. Oh, A. Alspach, R.J. Gross, and JunHo Oh. ”a common interface for humanoid simulation and hardware”. In *Humanoid Robots (Humanoids), 2010 10th IEEE-RAS International Conference on*, pages 587–592, 2010.

- [13] E. Gambao and C. Balaguer. "robotics and automation in construction". In *IEEE Robotics and Automation Magazine*. IEEE-IARP, 2002.
- [14] K. Tanie K. Yokoi S. Hirai H. Hirukawa K. Hirai S. Nakayama K. Sawada T. Nishiyama O. Miki T. Itoko H. Inaba H. Inoue, S. Tachi and M. Sudo. "hrp: Humanoid robotics project of mit". In *Proc. IEEE- RAS Int. Conf. Humanoid Robots, 2000*. IEEE-RAS, 2000.
- [15] W. R. Hamel and P. Murray. "observations concerning Internet-based teleoperations for hazardous environments". In *Proc. of 2001 IEEE Int. Conf on Robotics and Automation*, 2001.
- [16] H. Hasunuma, M. Kobayashi, H. Moriyama, T. Itoko, Y. Yanagihara, T. Ueno, K. Ohya, and K. Yokoi. "a tele-operated humanoid robot drives a lift truck". In *Robotics and Automation, 2002. Proceedings. ICRA '02. IEEE International Conference on*, volume 3, pages 2246–2252, 2002.
- [17] H. Hasunuma and K. Nakashima. "the tele-operation of the humanoid robot - workspace extension of the arm with step motion". In *Humanoid Robots, 2005 5th IEEE-RAS International Conference on*, pages 245–252, 2005.
- [18] H. Hasunuma, K. Nakashima, M. Kobayashi, F. Mifune, Y. Yanagihara, T. Ueno, K. Ohya, and K. Yokoi. "a tele-operated humanoid robot drives a backhoe". In *Robotics and Automation, 2003. Proceedings. ICRA '03. IEEE International Conference on*, volume 3, pages 2998–3004 vol.3, 2003.
- [19] Hirohisa Hirukawa, Fumio Kanehiro, Kenji Kaneko, Shuuji Kajita, Kiyoshi Fujiwara, Yoshihiro Kawai, Fumiaki Tomita, Shigeoki Hirai, Kazuo Tanie, Takakatsu Isozumi, Kazuhiko Akachi, Toshikazu Kawasaki, Shigehiko Ota, Kazuhiko Yokoyama, Hiroyuki Handa, Yutaro Fukase, Jun ichiro Maeda, Yoshihiko Nakamura, Susumu Tachi, and Hirochika Inoue. Humanoid robotics platforms developed in {HRP}. *Robotics and Autonomous Systems*, 48(4):165 – 175, 2004. [jce:title;Humanoids 2003;/ce:titlej](#).
- [20] R. A. Jarvis. "sensor rich teleoperation of an excavating machine". In *IEEE Robotics and Automation Magazine*. IEEE-Field and Service Robotics, 1999.
- [21] K. Kaneko. "towards emergency response humanoid robots". In *Mechatronics (MECATRONICS) , 2012 9th France-Japan 7th Europe-Asia Congress on and Research and Education in Mechatronics (REM), 2012 13th Int'l Workshop on*, pages 504–511, 2012.
- [22] M. Likhachev. Ros search-base planning library stack [online]. available: <http://www.ros.org/wiki/sbp>. 2013.
- [23] Yuepin Lu, Qiang Huang, Min Li, XiaoYu Jiang, and M. Keerio. "a friendly and human-based teleoperation system for humanoid robot using joystick". In

- Intelligent Control and Automation, 2008. WCICA 2008. 7th World Congress on*, pages 2283–2288, 2008.
- [24] K.Conley J.Faust T.Foote J.Leibs E.Berger R.Wheeler M.Quigley, B.Gerkey and A.Ng. "ros:an open-source robot operating system". In *Proc. ICRA workshop on Open-Source Software*, 2009.
- [25] Richard A. Newcombe, Andrew J. Davison, Shahram Izadi, Pushmeet Kohli, Otmar Hilliges, Jamie Shotton, David Molyneaux, Steve Hodges, David Kim, and Andrew Fitzgibbon. "kinectfusion: Real-time dense surface mapping and tracking".
- [26] R. O’Flaherty, P. Vieira, M.X. Grey, P. Oh, A. Bobick, M. Egerstedt, and M. Stilman. "humanoid robot teleoperation for tasks with power tools". In *Technologies for Practical Robot Applications (TePRA), 2013 IEEE International Conference on*, pages 1–6, 2013.
- [27] Mikhail Pivtoraiko and Alonzo Kelly. Generating near minimal spanning control sets for constrained motion planning in discrete state spaces. In *Proceedings of the 2005 IEEE/RSJ International Conference on Intelligent Robots and Systems (IROS '05)*, pages 3231 – 3237, August 2005.
- [28] Tianmiao Wang Qiang Huang, Kejie Li. "control and mechanical design of humanoid robot bhr-01". In *Proceeding of The Third IARP International Workshop on Humanoid and Human Friendly Robotics*. IEEE-IARP, 2002.
- [29] C. Rasmussen, K. Yuvraj, R. Vallett, Kiwon Sohn, and P. Oh. "towards functional labeling of utility vehicle point clouds for humanoid driving". In *Technologies for Practical Robot Applications (TePRA), 2013 IEEE International Conference on*, pages 1–6, 2013.
- [30] Radu Bogdan Rusu and Steve Cousins. "3d is here: Point cloud library (pcl)". In *International Conference on Robotics and Automation*, Shanghai, China, 2011 2011.
- [31] et al S. E. Salcudean. "bilateral matched impedance teleoperation with application to exca- vator control". In *Proc. of 1998 IEEE 1111. Conf on Robotics and Aufomation*, 1998.
- [32] M. Stilman, K. Nishiwaki, and S. Kagami. "humanoid teleoperation for whole body manipulation". In *Robotics and Automation, 2008. ICRA 2008. IEEE International Conference on*, pages 3175–3180, 2008.
- [33] C.E. Thorpe. "vision and navigation the camegie mellon navlab". In *Kluwer Academic Publishers*, 1990.

- [34] K. Yokoi, K. Nakashima, M. Kobayashi, H. Mihune, H. Hasunuma, Y. Yanagihara, T. Ueno, T. Gokyyu, and K. Endou. "a tele-operated humanoid robot drives a backhoe in the open air". In *Intelligent Robots and Systems, 2003. (IROS 2003). Proceedings. 2003 IEEE/RSJ International Conference on*, volume 2, pages 1117–1122 vol.2, 2003.
- [35] Lei Zhang, Qiang Huang, Yuepin Lu, Tao Xiao, Jiapeng Yang, and M. Keerio. "a visual tele-operation system for the humanoid robot bhr-02". In *Intelligent Robots and Systems, 2006 IEEE/RSJ International Conference on*, pages 1110–1114, 2006.

